

A laser-driven mixed fuel nuclear fusion micro-reactor concept

Hartmut Ruhl and Georg Korn

Marvel Fusion, Blumenstrasse 28, Munich, Germany

Abstract

We propose a laser-driven near-solid density nano-structured micro-reactor concept operating with mixed nuclear fusion fuels. The micro-reactor is capable of making use of a range of neutronic and aneutronic fuels. Its core parts consists of an embedded nanoscopic nuclear fuel based laser-driven nano-accelerator that is capable of producing non-thermal fuel distributions almost instantly.

Keywords: integrated accelerator, nanoscopic reactor, nanoscopic converter, nonlinear optics, secular field generator, non-thermal Lawson criteria

Contents

1	Introduction to the concept	1
2	The abstraction model	2
3	Rate equations for reactions	2
4	The integrated nano-accelerator	4
5	Conversion fraction	6
6	Nonlinear optics	8
7	Radiative energy loss	10
8	Summary	10
9	Acknowledgements	11

1. Introduction to the concept

In recent years there has been an abundance of papers in the field of ultra-short ultra-intense laser-matter interaction with nano-structures. We quote [1, 2, 3] and the literature therein to give examples.

Since lasers represent the fastest macroscopic energy sources we propose a micro-reactor powered by ultra-short ultra-high intensity laser pulses with UV to VUV wavelengths. Nano-structures promise an efficient way of transferring laser energy into a target. Simulations show that near complete laser deposition in nano-structured targets is possible.

With the help of the conversion fraction η^{kl} , which is defined later in the paper, modes of operation of the micro-reactor and their limits can be discussed and linked to existing experiments. In addition, with the help of η^{kl} it is possible to identify fusion conversion enhancing configurations.

Many of the papers in the field discuss nano-structures that are either extremely small and randomly oriented or the structures are so large that they cannot be called nano-structures anymore. Here, we propose a nano-structured nuclear micro-reactor with comparatively small structures size, which is entirely composed of nuclear fuels.

It comprises an integrated nano-structured accelerator consisting of boron or lithium rods with structure radii of $R \leq 30$ nm doped with constituents of nuclear fuels. The nuclear fuels can have a range of Gamov energies and S -factors. They can be neutronic or aneutronic or any mix of the latter. There are interesting chemical compounds like lithium borohydrate, that have very high natural densities for these nuclear fuel constituents.

The nano-rods are supposed to ionize rapidly leading to subsequent fuel releasing Coulomb explosions propagating close to the speed of light along the laser pulse. Coulomb explosions are efficient if electronic recurrence into the ionizing nano-structures is avoided. In addition, ultra-short high energy laser pulses are capable of over-heating electrons thus reducing electronic collisionality.

The purpose of the present paper is to outline the nano-structured micro-reactor concept, the abstraction model, and to discuss some of its properties, modes of operation, and its limitations on a parametric level.

The paper is structured in the following way. In section 2 the abstraction model is outlined for future reference. In section 3 simplified relativistic transport equations are discussed in preparation of the numerical model in future versions of this paper. With the help of the relativistic transport equations the parameters required for high fusion efficiency can be identified. In section 4 the concept of the embedded nano-accelerator is introduced. In section 5 the conversion fraction and efficiency are addressed. In section 6 the laser parameters required for the desired optical properties of the laser pulses interacting with nano-rods are sketched. In section 7 radiative energy loss processes are addressed.

2. The abstraction model

Since the required laser pulse radiation is ultra-intense electrons will become relativistic. There might also be positrons. Hence, we refer to [4, 5, 6, 7]. For future reference we state an expansion into a quantum BBGKY-hierarchy up to binary correlation order in the presence of electromagnetic fields leads to

$$\begin{aligned}
& \left(p_k^\mu \frac{\partial}{\partial x^\mu} + m_k F_k^i \frac{\partial}{\partial p_k^i} \right) f(x, \vec{p}_k) \\
&= \sum_{l, k', l'} \int \frac{d^3 p_l}{p_l^0} \frac{d^3 p_{l'}}{p_{l'}^0} \frac{d^3 p_{k'}}{p_{k'}^0} \\
&\quad \times \mathcal{A}(p_l p_k, p_{k'}, p_{l'}) f(x, \vec{p}_{l'}) f(x, \vec{p}_{k'}) \\
&\quad - \sum_{l, k', l'} \int \frac{d^3 p_l}{p_l^0} \frac{d^3 p_{k'}}{p_{k'}^0} \frac{d^3 p_{l'}}{p_{l'}^0} \\
&\quad \times \mathcal{A}(p_{l'} p_{k'}, p_k p_l) f(x, \vec{p}_k) f(x, \vec{p}_l),
\end{aligned} \tag{1}$$

where the invariant transition amplitude is given by

$$\begin{aligned}
& \mathcal{A}(p_l p_k, p_{k'}, p_{l'}) \\
&= \delta^4(p_l + p_k - p_{l'} - p_{k'}) \left| \langle p_l p_k | \mathcal{T}_{in} | p_{k'} p_{l'} \rangle \right|^2.
\end{aligned} \tag{2}$$

The binary \mathcal{T}_{in} -matrix in (2) has to be calculated in the context of ultra-strong electromagnetic fields. Hence, appropriately dressed states are required. Calculations of that kind in a somewhat different context are found in [8]. The \mathcal{T}_{in} -matrix is obtained with the help of the \mathbf{S}_{in} -matrix, which is to lowest order

$$\mathbf{S}_{in} = \mathbb{1} + \frac{1}{\hbar c} \int_{-\infty}^{\infty} d^4 x : \mathcal{L}_I^{in}(x) : . \tag{3}$$

This implies

$$\begin{aligned}
& {}_{in} \langle q_1 q_2 | \mathbf{S} - \mathbb{1} | p_2 p_1 \rangle_{in} \\
&= \frac{i}{\hbar c} (2\pi\hbar)^4 \delta^4(p_1 + p_2 - q_1 - q_2) \\
&\quad \times {}_{in} \langle q_1 q_2 | : \mathcal{L}_I^{in} : | p_2 p_1 \rangle_{in}
\end{aligned} \tag{4}$$

and hence

$$\begin{aligned}
& \langle q_1 q_2 | \mathcal{T} | p_2 p_1 \rangle \\
&= \frac{2\pi}{c} (2\pi\hbar)^4 {}_{in} \langle q_1 q_2 | : \mathcal{L}_I^{in} : | p_2 p_1 \rangle_{in}.
\end{aligned} \tag{5}$$

In section 3 we give details of the abstraction model based on the general relativist structure of the transport equations stated here.

3. Rate equations for reactions

The abstraction model (1) - (5) contains the dynamics of all particles embedded in a self-consistent electromagnetic field context inside the convertor as depicted in Fig. 1. It is also the basis of the numerical abstraction model in future papers.

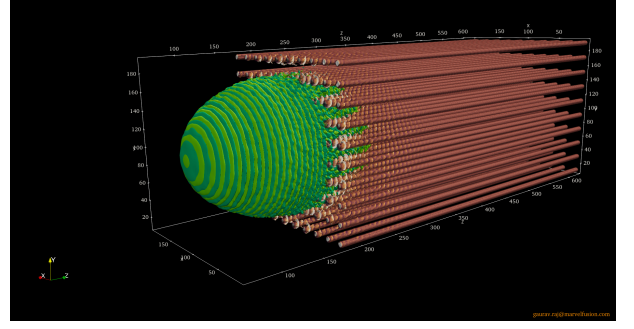


Figure 1: Cylindrical boron nano-rods with $R \leq 30$ nm are placed inside the micro-reactor. The boron nano-rods contain protons, deuterons, and tritium. An ultra-short high intensity UV laser pulse impinges on the reactor from the left and couples to the boron nano-rods. The nano-structured absorber extends beyond the laser focal spot in lateral directions.

This is one reason why we state the details of it here. We will also make use of it later in the paper.

A fusing kl -system can be approximately described by the following kinetic equations

$$\begin{aligned}
& p_k^\mu \frac{\partial f_k}{\partial x^\mu} + m_k F_k^i \frac{\partial f_k}{\partial p_k^i} \\
&= \sum_{l, k', l'} \int \frac{d^3 p_l}{p_l^0} \int \frac{d^3 p_{k'}}{p_{k'}^0} \int \frac{d^3 p_{l'}}{p_{l'}^0} \\
&\quad \times (W_{klk'l'}^C f_{k'} f_{l'} - W_{k'l'kl}^C f_k f_l) \\
&\quad - \sum_{l, k', l'} \int \frac{d^3 p_l}{p_l^0} \int \frac{d^3 p_{k'}}{p_{k'}^0} \int \frac{d^3 p_{l'}}{p_{l'}^0} W_{k'l'kl}^R f_k f_l
\end{aligned} \tag{6}$$

and

$$F_k^\mu = \frac{q_k}{m_k c} F^{\mu\nu} p_{k\nu}, \tag{7}$$

where the q_k are the electric charges of particles k and $F^{\mu\nu}$ is the electric field strength tensor. Maxwell's equations are given by

$$\frac{\partial}{\partial x^\mu} F^{\mu\nu} = \frac{j^\nu}{c^2 \epsilon_0}, \quad \frac{\partial}{\partial x^\mu} \tilde{F}^{\mu\nu} = 0, \tag{8}$$

where $\tilde{F}^{\mu\nu}$ is the dual of $F^{\mu\nu}$. The total four current is

$$j^\nu = \sum_k q_k \int d^4 p \, 2\Theta(p_0) \delta(p^2 - m_k^2 c^2) c p^\nu f_k, \tag{9}$$

where the collisional and reactive invariant transition amplitudes W^C and W^R can be mapped onto invariant collisional and reactive cross sections σ_C and σ_R provided the underlying system is sufficiently dilute and weakly coupling with the help of

$$W_{klk'l'}^C = W_{k'l'kl}^C, \tag{10}$$

$$W_{k'l'kl}^C = s \sigma_C^{kl}(s, \psi) \delta^4(p_{k'} + p_{l'} - p_k - p_l) \delta_{k'k} \delta_{l'l}, \tag{11}$$

$$W_{k'l'kl}^R = s \sigma_R^{kl}(s, \psi) \delta^4(p_{k'} + p_{l'} - p_k - p_l), \tag{12}$$

$$s = (p_k^\mu + p_l^\mu)^2.$$

The kinematics of the reactions in the kl -system is best analyzed in the center of mass frame

$$\vec{p}_k^{cm} = \vec{p}_k + \frac{1}{\beta^2} (\gamma - 1) (\vec{p}_k \cdot \vec{\beta}) \vec{\beta} - \gamma \vec{\beta} p_k^0, \quad (13)$$

$$\vec{p}_l^{cm} = \vec{p}_l + \frac{1}{\beta^2} (\gamma - 1) (\vec{p}_l \cdot \vec{\beta}) \vec{\beta} - \gamma \vec{\beta} p_l^0,$$

where

$$\vec{\beta} = \frac{\vec{p}_k + \vec{p}_l}{p_k^0 + p_l^0}, \quad (14)$$

$$\gamma = \frac{1}{\sqrt{1 - \beta^2}}, \quad (15)$$

$$p_k^0 = \sqrt{m_k^2 c^2 + \vec{p}_k^2}, \quad (16)$$

$$p_l^0 = \sqrt{m_l^2 c^2 + \vec{p}_l^2}. \quad (17)$$

The quantity p is the length of the CM-frame momenta \vec{p}_k^{cm} and \vec{p}_l^{cm} . It is given by

$$p = \frac{1}{2\sqrt{s}} \sqrt{(s - (m_k^2 + m_l^2) c^2)^2 - 4 m_k^2 m_l^2 c^4}. \quad (18)$$

To define the post-collision momenta we introduce a right-handed coordinate system in the CM frame, the \vec{e}_1 -axis of which is along \vec{p}_k^{cm} . The CM frame coordinate system is embedded into a right-handed coordinate system in the lab frame. The z -axis of the latter is along \vec{e}_z . For the parametrization of

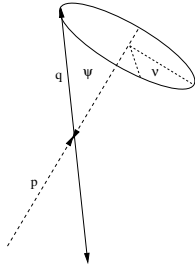


Figure 2: Release angles of nuclear fusion products for binary decays.

the nuclear fusion products in the $k'l'$ -system the angles ψ and ν are introduced as indicated in Fig. 2. We construct three orthonormal vectors for all three coordinate axes as follows

$$\vec{e}_1 = \frac{\vec{p}_k^{cm}}{|\vec{p}_k^{cm}|}, \quad (19)$$

$$\vec{e}_2 = \frac{\vec{p}_k^{cm} \times \vec{e}_z}{|\vec{p}_k^{cm} \times \vec{e}_z|}, \quad (20)$$

$$\vec{e}_3 = \frac{(\vec{p}_k^{cm} \times \vec{e}_z) \times \vec{p}_k^{cm}}{|(\vec{p}_k^{cm} \times \vec{e}_z) \times \vec{p}_k^{cm}|}. \quad (21)$$

If $s \geq (m_k c + m_l c)^2$ holds, where $m_{k'}$ and $m_{l'}$ denote either the post-collisional masses or the masses of the binary nuclear

fusion products, we can calculate the post-collisional or post-fusion momenta in the CM-frame

$$p_{k'}^{0,cm} = \sqrt{m_{k'}^2 c^2 + q^2}, \quad (22)$$

$$\vec{p}_{k'}^{cm} = q \cos \psi \vec{e}_1 + q \sin \psi \sin \nu \vec{e}_2 + q \sin \psi \cos \nu \vec{e}_3, \quad (23)$$

$$p_{l'}^{0,cm} = \sqrt{m_{l'}^2 c^2 + q^2}, \quad (24)$$

$$\vec{p}_{l'}^{cm} = -\vec{p}_{k'}^{cm}, \quad (25)$$

where q is given by

$$q = \frac{1}{2\sqrt{s}} \sqrt{(s - (m_{k'}^2 + m_{l'}^2) c^2)^2 - 4 m_{k'}^2 m_{l'}^2 c^4}. \quad (26)$$

Finally we transform back into the lab-frame. Since the CM frame moves with the velocity $c\vec{\beta}$ we can go back to the lab frame by boosting the CM frame with the velocity $-c\vec{\beta}$. We obtain for the post-collision variables in the lab frame

$$p_{k'}^0 = \gamma (p_{k'}^{0,cm} + \vec{\beta} \cdot \vec{p}_{k'}^{cm}), \quad (27)$$

$$\vec{p}_{k'} = \vec{p}_{k'}^{cm} + \frac{1}{\beta^2} (\gamma - 1) (\vec{p}_{k'}^{cm} \cdot \vec{\beta}) \vec{\beta} + \gamma \vec{\beta} p_{k'}^{0,cm}, \quad (28)$$

$$p_{l'}^0 = \gamma (p_{l'}^{0,cm} + \vec{\beta} \cdot \vec{p}_{l'}^{cm}), \quad (29)$$

$$\vec{p}_{l'} = \vec{p}_{l'}^{cm} + \frac{1}{\beta^2} (\gamma - 1) (\vec{p}_{l'}^{cm} \cdot \vec{\beta}) \vec{\beta} + \gamma \vec{\beta} p_{l'}^{0,cm}. \quad (30)$$

At this point we have the momenta of the nuclear fusion products in the $k'l'$ -system in the lab frame again. We note that the masses of the products are typically different. However, total energy and momentum are conserved.

Since electrons are relativistic and to derive simple scaling laws for nuclear fusion efficiency at a later point in this paper three notations are helpful. The three notation are obtained by performing the integration over $\vec{p}_{l'}$ in (6). We obtain $\vec{p}_{l'} = \vec{p}_k + \vec{p}_l - \vec{p}_{k'}$. Making use of the center of mass frame we find

$$\frac{\delta (p_k^{0,cm} + p_l^{0,cm} - p_{k'}^{0,cm} - p_{l'}^{0,cm})}{p_{k'}^{0,cm} p_{l'}^{0,cm}} \quad (31)$$

$$= \frac{\delta (|\vec{p}_{k'}^{cm}| - \frac{\mathcal{F}_{kl}}{\sqrt{s}})}{|\vec{p}_{k'}^{cm}| \sqrt{s}},$$

where the quantity \mathcal{F}_{kl} is given by

$$\mathcal{F}_{kl} = \sqrt{(p_k \cdot p_l)^2 - m_k^2 m_l^2 c^4}. \quad (32)$$

In the velocity space this leads to

$$\begin{aligned} & \frac{\partial f_k}{\partial t} + \vec{v}_k \cdot \frac{\partial f_k}{\partial \vec{x}_k} + q_k (\vec{E} + \vec{v}_k \times \vec{B}) \cdot \frac{\partial f_k}{\partial \vec{p}_k} \\ &= \sum_l \int d^3 p_l v_{rel}^{kl} \int d\Omega_\psi \sigma_C^{kl}(s, \psi) (f_{l'} f_{k'} - f_l f_k) \\ & - \sum_l \int d^3 p_l v_{rel}^{kl} \int d\Omega_\psi \sigma_R^{kl}(s, \psi) f_k f_l, \end{aligned} \quad (33)$$

where

$$v_{rel}^{kl} = \frac{c \mathcal{F}_{kl}}{p_k^0 p_l^0} = \sqrt{|\vec{v}_k - \vec{v}_l|^2 - \frac{1}{c^2} (\vec{v}_k \times \vec{v}_l)^2}, \quad (34)$$

$$\vec{v}_k = \frac{c \vec{p}_k}{\sqrt{m_k^2 c^2 + \vec{p}_k^2}}. \quad (35)$$

We finally find

$$\begin{aligned} & \frac{\partial f_k}{\partial t} + \vec{v}_k \cdot \frac{\partial f_k}{\partial \vec{x}_k} + \frac{q_k}{m_k} (\vec{E} + \vec{v}_k \times \vec{B}) \cdot \frac{\partial f_k}{\partial \vec{v}_k} \\ &= \sum_l \int d^3 v_l v_{rel}^{kl} \int d\Omega_\psi \sigma_C^{kl}(s, \psi) (f_l' f_k' - f_l f_k) \\ & \quad - \sum_l \int d^3 v_l v_{rel}^{kl} \int d\Omega_\psi \sigma_R^{kl}(s, \psi) f_k f_l, \end{aligned} \quad (36)$$

where fuel breeding is excluded.

In section 4 we parametrically discuss the integrated nanoscopic accelerator concept. It relies on the assumption that the driver laser is capable of removing sufficiently many electrons from the nano-rods in the micro-reactor in a predictable way. We will not investigate the details in this paper and leave it for future numerical analysis.

4. The integrated nano-accelerator

We assume that energy transfer to fuel constituents takes place with the help of the electromagnetic fields of the driver laser. This energy delivery system has a chance to be efficient and fast for almost all nuclear fusion fuels.

The convertor concept discussed in the present paper consists of a laser-powered integrated nano-structured accelerator. For reasons of efficiency it consists exclusively of very small nuclear fuel based nano-structures that allow Coulomb explosions.

The integrated nano-accelerator is assumed to be an efficient design for the generation of large ionic currents at low ion energies. It is powered by ultra-short ultra-high energy laser pulses in the UV to the VUV wavelength range. The integrated accelerator is expected to absorb the driver laser energy almost completely avoiding parametric optical instabilities.

Nano-structures can be efficient laser energy convertors into ionic motion if the electrons in the nano-structures can be over-heated by the driver laser. Over-heated electrons are those that cannot be recaptured by the ionized nano-structures within the time window the Coulomb explosions take. Hence, positive ions are exposed to their own electric space-charge field for long enough and Coulomb explode, leaving behind after some time, a nearly homogeneous ionic distribution in configuration space and a non-thermal one in the momentum space that can be engineered such that it is peaked at the resonances of the provided nuclear fuel mix.

Specifically, we consider cylindrical nano-rods that form the embedded nano-accelerator as sketched in Fig. 1, which is composed of rigid fuel constituents l into which lighter fuel constituents k are embedded. We assume $e_l/m_l \ll e_k/m_k$ for the effective charges and fuel masses involved. Between accelerator

nano-rods low Gamov energy fuel ions can be placed in form of foams. Since we propose UV to VUV driver laser wavelengths we assume that the laser is still capable of propagating through the proposed convertor in a stable and predictable way.

The VUV laser driver ionizes the nano-rods partially. The ionizing electrons occupy the space inside and between the nano-rods in such a way that individual nano-rods are partially shielded from each other. Still they provide an ion accelerating electric field strong enough to obtain the required relative energies between the fuel constituents for the provided fusion resonances of the fuel mix.

For reasons of simplicity we make the following assumption for the electric field of a single nano-rod composed of the high density fuel constituent l

$$E_r(r_k) = \begin{cases} C_l r_k, & 0 \leq r_k < R \\ 0, & r_k \geq R \end{cases}, \quad C_l = \frac{e n_l}{2 \epsilon_0}, \quad (37)$$

where the nanoscopic field E_r is radial and n_l represents the average positive charge density inside the rods. The parameter r_k is the radial position of an ion of sort k inside the nano-rod composed of ions of sort l and R is the nano-rod radius.

Since collisions and fusion reactions are rare on fs time scales, which the postulated Coulomb explosions require, we neglect the collision and fusion operators in (36) during the Coulomb explosion phase. In addition, we assume that the light ions only expand radially, while the heavy ones stand still. Hence, for $r_k \leq R$ the acceleration of the k -ions is approximated by the following radial Vlasov equation

$$\left(\partial_t + v_k \partial_{r_k} + \frac{e_k}{m_k} C_l r_k \partial_{v_k} \right) (r_k v_k f_k)(r_k, v_k, t) = 0, \quad (38)$$

where f_k now is a distribution function in polar coordinates. The above approximation is justified for the $p^{11}\text{B}$ fuel, for example. For $r_k > R$ the light ions undergo further acceleration. Also the heavy ions l are ultimately subject to acceleration. However, for simplicity we neglect secondary forces on all fuel ions kl . This implies for the light ions of sort k for $r_k > R$

$$(\partial_t + v_k \partial_{r_k}) (r_k v_k f_k)(r_k, v_k, t) = 0 \quad (39)$$

until they collide or fuse.

According to (38) the light ions fulfill the following equations of motion during the Coulomb explosion phase

$$\frac{dr_k}{dt} = v_k, \quad \frac{dv_k}{dt} = \frac{e_k}{m_k} C_l r_k, \quad (40)$$

while the solution of (38) is

$$(r_k v_k f_k)(r_k, v_k, t) = (r_{k0} v_{k0} f_k)(r_{k0}, v_{k0}, 0), \quad (41)$$

where due to (40) we have

$$\begin{pmatrix} r_{k0} \\ v_{k0} \end{pmatrix} = \begin{pmatrix} \cosh\left(\sqrt{\frac{e_k C_l}{m_k}} t\right) & -\frac{1}{\sqrt{\frac{e_k C_l}{m_k}}} \sinh\left(\sqrt{\frac{e_k C_l}{m_k}} t\right) \\ -\sqrt{\frac{e_k C_l}{m_k}} \sinh\left(\sqrt{\frac{e_k C_l}{m_k}} t\right) & \cosh\left(\sqrt{\frac{e_k C_l}{m_k}} t\right) \end{pmatrix} \begin{pmatrix} r_k \\ v_k \end{pmatrix}. \quad (42)$$

The parameter $r_{k0} \leq R$ is the initial radial position of the light ions and $v_{k0} > 0$ their initial radial velocity. The parameters r_k and v_k are the radial position and velocity at times $t > 0$.

To estimate the energy distribution of the light ions we consider a layer s of the latter with initial radial position $0 < r_k^s(0) \leq R$ and a radial velocity distribution given by

$$\begin{aligned} & (r_{k0} v_{k0} f_k)(r_{k0}, v_{k0}, 0) \\ &= \frac{N_k^s}{4\pi^2} \delta(r_{k0} - r_k^s(0)) \delta(v_{k0} - v_k^s(0)), \end{aligned} \quad (43)$$

where N_k^s is the initial number of particles k at the radial position $r_k^s(0)$. Plugging r_{k0} and v_{k0} given by (42) into (43) assuming $v_k^s(0) = 0$ gives for $t \leq t_k^s$

$$r_k v_k f_k^s(r_k, v_k, t) = \frac{N_k^s}{4\pi^2} \delta(r_k - r_k^s(t)) \delta(v_k - g_k^s(t)), \quad (44)$$

where

$$t_k^s = \sqrt{\frac{m_k}{e_k C_l}} \cosh^{-1} \left(\frac{R}{r_k^s(0)} \right), \quad (45)$$

$$r_k^s(t) = r_k^s(0) \cosh \left(\sqrt{\frac{e_k C_l}{m_k}} t \right), \quad (46)$$

$$g_k^s(t) = \sqrt{\frac{e_k C_l}{m_k}} r_k^s(0) \sinh \left(\sqrt{\frac{e_k C_l}{m_k}} t \right). \quad (47)$$

After rapid acceleration during the Coulomb explosion phase the light ion layer is assumed to move on ballistically. At t_k^s we obtain

$$r_k v_k f_k^s(r_k, v_k, t_k^s) = \frac{N_k^s}{4\pi^2} \delta(r_k - r_k^s(t_k^s)) \delta(v_k - g_k^s(t_k^s)), \quad (48)$$

where

$$r_k^s(t_k^s) = R, \quad (49)$$

$$g_k^s(t_k^s) = \sqrt{\frac{e_k C_l}{m_k}} \sqrt{R^2 - (r_k^s(0))^2}. \quad (50)$$

It holds that

$$(2\pi)^2 \int_0^\infty dv_k v_k \int_0^\infty dr_k r_k f_k^s(r_k, v_k, t) = N_k^s. \quad (51)$$

Simulations confirm that an approximately homogeneous and isotropic light ion distribution in configuration space is obtained after the interaction with the laser pulse, while a peaked non-thermal light ion distribution in momentum space remains. Figure 3 shows a simulation of the laser impinging on the nanostructures, which extend beyond the interaction volume with the laser. Figure 4 shows the proton momentum and Fig. 5 the boron momentum distribution obtained from the same simulation. The distribution function f_p of the protons is peaked at small momenta mainly due to rods not interacting with the laser pulse and at $|\vec{p}_p| \approx 0.03 m_p c$ due to nano-acceleration and periodic boundaries used in configuration space. There are also many protons at $|\vec{p}_p| > 0.05 m_p c$.

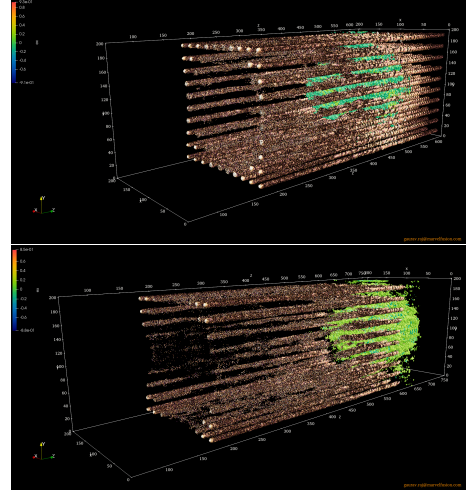


Figure 3: The laser impinges on the nano-reactor from the left. Two time frames are shown. The box size is $8 \mu\text{m} \times 8 \mu\text{m} \times 32 \mu\text{m}$. The nano-rods are 30 nm wide and about 800 nm apart. The laser wavelength is 250 nm. The laser is circularly polarized. The laser driver has nearly constant loss of energy per unit of propagation length. The laser does not self-focus. It captures electrons forming a magnetic field that separates electron current and return currents. The plot shows that the plasma starts to pinch. The simulation is the same as the one in Fig. 1.

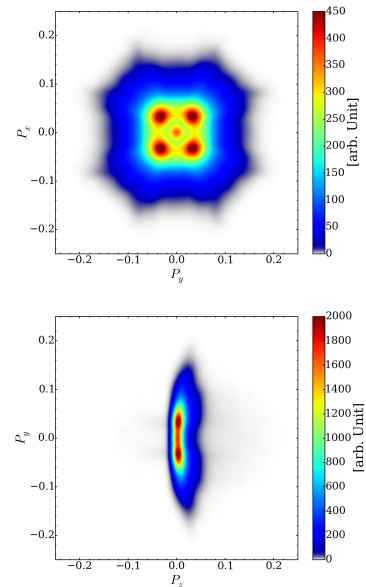


Figure 4: Proton momentum distributions integrated over the configuration space after the laser pulse has exited the nano-structures. The proton momenta are normalized to $m_p c$. The simulation has lateral periodic boundaries, while the laser pulse is a central disk with 10 fs pulse length and $\lambda = 250$ nm. The polarization is circular. The simulation is the same as the one in Fig. 1.

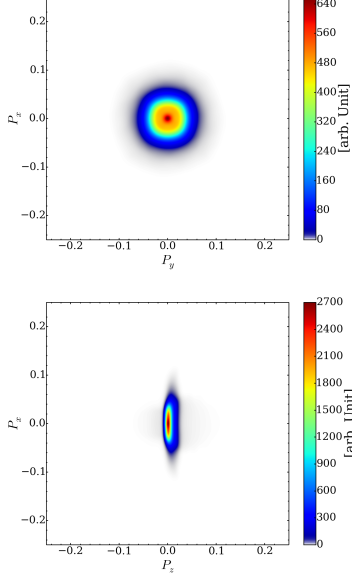


Figure 5: Boron momentum distributions integrated over the configuration space after the laser pulse has exited the nano-structures. The boron momenta are normalized to m_{Bc} . The simulation has lateral periodic boundaries, while the laser pulse is a central disk with 10 fs pulse length and $\lambda = 250$ nm. The polarization is circular. The simulation is the same as the one in Fig. 1.

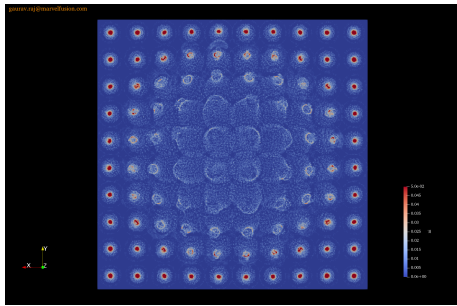


Figure 6: Coulomb explosions in the body of the laser pulse. The explosion front propagates with almost the speed of light. The simulation is the same as the one in Fig. 1.

5. Conversion fraction

To derive a relation for the burn fraction we make use of (36). Next, we need parametrizations of the ionic distribution functions. We assume that the ions of sort k are mobile and make the ansatz

$$f_k(\vec{r}_k, \vec{v}_k, t) \approx \sum_{i,s} \alpha_k^s N_k^i(t) \delta^3(\vec{r}_k - \vec{r}_k^{s,i}(t)) \delta^3(\vec{v}_k - \vec{g}_k^{s,i}(t)). \quad (52)$$

We further assume that the ions of sort l are immobile. We make the ansatz

$$f_l(\vec{r}_l, \vec{v}_l, t) \approx \frac{N}{V} \sum_i N_k^i(t) \delta^3(\vec{v}_l). \quad (53)$$

Summation over all fluid elements i implies

$$N_k = \sum_i N_k^i, \quad (54)$$

$$n_l(t) = n_k(t) = \frac{N}{V} N_k(t). \quad (55)$$

In addition we have

$$\alpha_k^s = \frac{2r_k^s(0) \Delta r_k}{R^2}, \quad (56)$$

$$\sum_s \alpha_k^s = 1. \quad (57)$$

The parameter N is the number of nano-rods in the reactor, that can be reached by the accelerated fuel constituent k , and Δr_k is the thickness of the layer s_k of the fuel constituent k in a single nano-rod. We assume that all initial velocity directions of constituent k are uniformly distributed while their absolute velocity values are given by (50). The initial positions are determined by the positions of the nano-rods. In addition, each velocity group of constituent k has its own density group. All density groups of constituent k add up to the total density.

Intra-ionic collision do not drain much energy from the ionic subsystem. They predominantly redistribute phase-space without much energy loss. Hence, we neglect them. Electron - ion collisions, however, do not change the direction of the ions very much, but are potentially capable of draining a lot of energy from the ions. Assuming an adequate shape of the electronic distribution function f_e the collision integral in (36) leads to resistivities. We do not discuss further details here.

With the help of the zero and first order velocity moments of (36), neglecting the electromagnetic fields in (36), making use of (52) - (57) and our assumption about the electronic distribution function we obtain for the ions of sort k of a single rod

$$\frac{dN_k^i(t)}{dt} \approx -N_k^i(t) N_k(t) \frac{N}{V} \sum_s \alpha_k^s g_k^{s,i}(t) \sigma_R^{kl}(g_k^{s,i}(t)), \quad (58)$$

where

$$\frac{d\vec{g}_k^{s,i}(t)}{dt} \approx -v_{ke}^{s,i}(g_k^{s,i}(t)) \vec{g}_k^{s,i}(t) \quad (59)$$

and

$$\frac{d\vec{g}_k^{s,i}(t)}{dt} = \vec{g}_k^{s,i}(t). \quad (60)$$

The $v_{ke}^{s,i}$ are the resistivities approximately given by

$$v_{ke}^{s,i}(\vec{g}_k^{s,i}(t)) \approx \frac{e_k^2 e^2 \frac{N}{V} N_k^i}{4\pi\epsilon_0^2 m_{ke}^2 |\vec{g}_k^{s,i}(t) - \vec{v}_e(t)|^3} \ln \Lambda_{ke}, \quad (61)$$

where \vec{v}_e is the electron velocity and $\ln \Lambda_{ke}$ is the Coulomb logarithm.

Equations (58) - (60) are quasi-element equations for fuel ions. As they are they cannot be solved. However, assuming that all nano-rods are the same and that there is rotational and translational invariance of the system the index i can be dropped and we obtain the much simpler system of equations

$$\frac{dN_k(t)}{dt} \approx -N_k^2(t) \frac{N}{V} \sum_s \alpha_k^s g_k^s(t) \sigma_R^{kl}(g_k^s(t)), \quad (62)$$

where

$$\frac{d\vec{g}_k^s(t)}{dt} \approx -v_{ke}^s(\vec{g}_k^s(t)) \vec{g}_k^s(t) \quad (63)$$

and

$$\frac{d\vec{v}_k^s(t)}{dt} = \vec{g}_k^s(t). \quad (64)$$

Mean field and binary level radiation loss effects are neglected in (63) - (64).

Equation (62) decouples from (63) and (64). It can be solved. We find

$$\Delta N_k \approx \frac{N_k}{1 + \frac{N}{V} N_k \int_{t_k^s}^{\infty} dt \sum_s \alpha_k^s g_k^s(t) \sigma_R^{kl}(g_k^s(t))}, \quad (65)$$

The parameter N_k is a free parameter. The conversion fraction is

$$\begin{aligned} \eta^{kl} &= 1 - \frac{\Delta N_k}{N_k} \\ &\approx \frac{\frac{N}{V} N_k \sum_s \alpha_k^s \int_{t_k^s}^{\infty} dt g_k^s(t) \sigma_R^{kl}(g_k^s(t))}{1 + \frac{N}{V} N_k \sum_s \alpha_k^s \int_{t_k^s}^{\infty} dt g_k^s(t) \sigma_R^{kl}(g_k^s(t))}. \end{aligned} \quad (66)$$

To obtain the velocity (63) has to be solved. We find

$$\vec{g}_k^s(t) = \vec{g}_k^s(t_k^s) e^{-v_{ke}^s(t-t_k^s)}, \quad t \gg t_k^s. \quad (67)$$

We assume that the fusion cross section is constant within a given velocity range

$$\sigma_R^{kl}(g_k^s(t)) = \begin{cases} \sigma_0^{kl}, & \sqrt{\frac{2\epsilon_G^{kl}}{m_k}} \leq g_k^s(t) \leq \sqrt{\frac{2\epsilon_G^{kl}}{m_k}} \\ 0, & \text{else} \end{cases}, \quad (68)$$

where σ_0^{kl} is the smallest value within the velocity range. A comparison of the cross sections for *DT* and *pB* is given in Fig. 7. It holds $\sigma_0^{DT,pB} \approx 10^{-28} \text{ m}^2$ for $0 < g_k^s(t) < 2 \cdot 10^7 \text{ ms}^{-1}$.

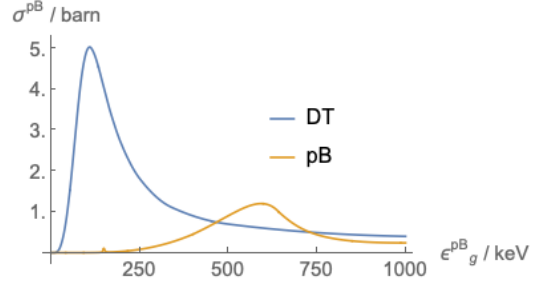


Figure 7: Comparison between the cross sections of pB and DT as quoted in reference [9].

There are many interesting fuel cycles from which σ_0^{kl} can be obtained. The cross sections can be parametrized as

$$\sigma_R^{kl}(g_k^s(t)) \approx \frac{S_{kl} \left(\frac{\epsilon_G^{kl}}{\beta_{av}^{kl}} \right)}{\epsilon_G^{kl}} \beta_{av}^{kl} e^{-\sqrt{\beta_{av}^{kl}}}, \quad (69)$$

where

$$\beta_{av}^{kl} = \frac{\epsilon_G^{kl}}{\epsilon_{av}^{kl}}, \quad (70)$$

$$\epsilon_{av}^{kl} = \frac{1}{2} m_{kl} (g_k^{av})^2, \quad (71)$$

$$\epsilon_G^{kl} = 2 \left(\frac{\pi e^2 Z_k Z_l}{4\pi\epsilon_0 \hbar c} \right)^2 m_{kl} c^2, \quad (72)$$

$$m_{kl} = \frac{m_k m_l}{m_k + m_l}. \quad (73)$$

The most relevant neutronic fuel cycles are given in table 1. They have small Gamov energies ϵ_G^{kl} and large S_{kl} . Advanced

standard fuels	ϵ_f^{kl} MeV	S_{kl} keV barn	$\sqrt{\epsilon_G^{kl}}$ $\sqrt{\text{keV}}$
D + T \rightarrow ${}^4\text{He} + \text{n}$	17.59	$1.2 \cdot 10^4$	34.38
D + D \rightarrow T + p	4.04	56.0	31.4
D + D \rightarrow ${}^3\text{He} + \text{n}$	3.27	54.0	31.4
D + D \rightarrow ${}^4\text{He} + \gamma$	23.85	$4.3 \cdot 10^{-3}$	31.4
T + T \rightarrow ${}^4\text{He} + 2\text{n}$	11.33	138.0	38.45

Table 1: Standard fuel cycles. They typically produce neutrons at high rates but are better suited for thermal nuclear fusion concepts.

fuel cycles are summarized in table 2. They have larger Gamov energies ϵ_G^{kl} than the neutronic fuel cycles. Hence, the cross sections are very small at low energies. At high energies, however, aneutronic fuel cycles become attractive as well. In particular, boron is a material that can be nano-fabricated and doped to form an integrated nano-accelerator. Protons, deuterons, and tritium can be implanted into boron.

We obtain

$$\sum_s \alpha_k^s \int_{t_k^s}^{\infty} dt g_k^s(t) \sigma_R^{kl}(g_k^s(t)) \approx \sigma_0^{kl} \sum_s \alpha_k^s \frac{g_k^s(t_k^s)}{v_{ke}^s}. \quad (74)$$

The exit velocities as a function of initial radius r_k^s are shown in Fig. 8. For appropriate nano-structures the exit velocity spread

advanced fuels	ϵ_f^{kl} MeV	S_{kl} keV barn	$\sqrt{\epsilon_G^{kl}} \sqrt{\text{keV}}$
$\text{D} + {}^3\text{He} \rightarrow {}^4\text{He} + \text{p}$	18.35	$5.9 \cdot 10^3$	68.75
$\text{p} + {}^6\text{Li} \rightarrow {}^4\text{He} + {}^3\text{He}$	4.02	$5.5 \cdot 10^3$	87.2
$\text{p} + {}^7\text{Li} \rightarrow 2{}^4\text{He}$	17.35	80.0	88.11
$\text{p} + {}^{11}\text{B} \rightarrow 3{}^4\text{He}$	8.68	$2.0 \cdot 10^5$	150.3

Table 2: Advanced fuel cycles. They typically produce less neutrons but have larger Gamov energies. Hence, cross sections are small at low energies making the fuel cycles difficult to trigger in a thermal context.

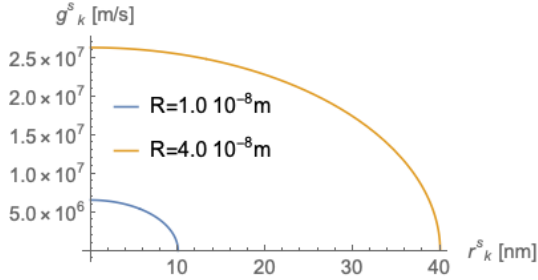


Figure 8: Exit velocities according to (50) as a function of initial radii. The nano-rod density is $n_l \approx 5 \cdot 10^{29} \text{ m}^{-3}$.

of the light ions k can be very small. With the help of an average exit velocity g_k^{av} we obtain

$$\eta^{kl} = \frac{n_l \mathcal{R}_k \sigma_0^{kl}}{1 + n_l \mathcal{R}_k \sigma_0^{kl}}, \quad \mathcal{R}_k \approx \frac{g_k^{av}}{\nu_{ke}}. \quad (75)$$

The parameter \mathcal{R}_k is the range of the fuel constituent k . Since the resistivities scale like the density n_l and the conversion fraction contains the product $n_l \mathcal{R}_k$, there is no dependence on the density n_l within the model outlined here. According to (61) and (75) the conversion efficiency η^{kl} limited by

$$\eta^{kl} < \frac{\frac{4\pi\epsilon_0^2 m_{ke}^2 c^3 g_k^{av} \sigma_R^{kl}}{\alpha e_k^2 e_e^2 \ln \Lambda_{ke}}}{1 + \frac{4\pi\epsilon_0^2 m_{ke}^2 c^3 g_k^{av} \sigma_R^{kl}}{\alpha e_k^2 e_e^2 \ln \Lambda_{ke}}}, \quad (76)$$

where $0 < \alpha < 1$ is the fraction of electrons divided by the number of ions in the volume of consideration. For the parameters

$$\alpha \approx 1, \quad \ln \Lambda_{ke} \approx 5, \quad \sigma_R^{kl} \approx 10^{-28} \text{ m}^2,$$

we have $\eta^{kl} < 0.02$. In the context there are many experiments dealing with pitcher - catcher configurations falling short of the approximate limit (76). The convertor proposed here represents an integrated pitcher - catcher configuration. It promises to be an order of magnitude more efficient than traditional pitcher - catcher configurations.

For simple situations η^{kl} depends on the $n_l \mathcal{R}_k$ product while n_l and \mathcal{R}_k are not independent of each other as (76) implies. To obtain a feeling for densities and ranges required for large conversion fractions we consider p^{11}B and DT.

For an average fuel density of about $n_B = n_p \approx 5.0 \cdot 10^{28} \text{ m}^{-3}$, an average velocity of $g_p^{av} \approx 2.0 \cdot 10^7 \text{ ms}^{-1}$ according to Fig. 8, and a resistivity of $\nu_{pe} \approx 10^{10} \text{ s}^{-1}$ the range is $\mathcal{R}_p \approx 2 \cdot 10^{-3} \text{ m}$

yielding $n_B \mathcal{R}_p \approx 10^{26} \text{ m}^{-2}$. The conversion fraction η^{pB} as a function of β_{av}^{pB} and $n_B \mathcal{R}_p$ is shown in Fig. 9.

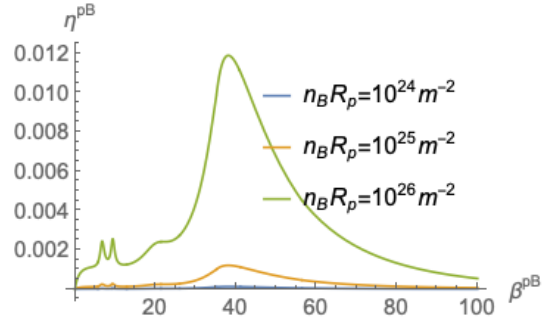


Figure 9: The expected conversion fraction η^{pB} as a function of β_{av}^{pB} and $n_B \mathcal{R}_p$ based on the cross section given in Fig. 7. Please note that according to (75) density and range are inversely proportional to each other. Values for the product $n_B \mathcal{R}_p$ can be obtained from (76).

For deuteron and tritium ions embedded within a boron nano-rod nano-acceleration is capable of generating energetic high density deuterons and tritium ions, which can collide with each other. The average density of the deuterium and tritium leaving the boron nano-rods can be as high as $n_D \approx 5 \cdot 10^{28} \text{ m}^{-3}$. The exit velocity of D is assumed to be 10^7 ms^{-1} , while the resistivity is $\nu_{De} \approx 10^{10} \text{ s}^{-1}$. We obtain $n_T \mathcal{R}_D \approx 10^{26} \text{ m}^{-2}$. The conversion fraction η^{DT} as a function of β_{av}^{DT} and $n_T \mathcal{R}_D$ is shown in Fig. 10.

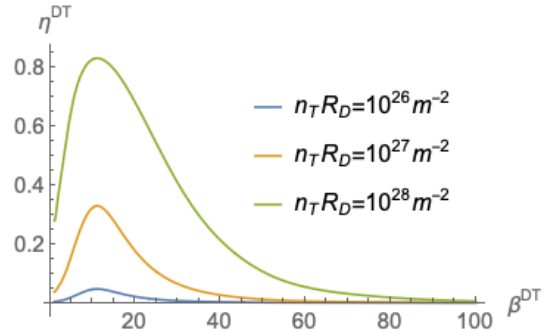


Figure 10: The expected conversion fraction η^{DT} as a function of β_{av}^{DT} and $n_T \mathcal{R}_D$. Please note that according to (75) density and range are inversely proportional to each other. Values for the product $n_T \mathcal{R}_D$ can be obtained from (76).

Since laser technology has made vast progress in recent years the exploration of fusion enhancing micro-configurations operating close to solid fuel density and at extremely high fuel energies with or without auto-catalysm is of great interest.

In section 6 some aspects of the nonlinear electron optical properties of the micro-reactor are addressed.

6. Nonlinear optics

Efficient embedded nano-acceleration of ions depends on specific optical properties of the laser driver interacting with the nano-structures.

The lower threshold for the electric field strength required to ionize the nano-rods to the charge density $e_i n_i$ is approximately

$$E \geq \frac{R}{e_e} \left(m_e \omega^2 + e_e C_l \right), \quad (77)$$

where ω is the laser frequency. The implication for the laser intensity is

$$I_c = \frac{1}{2} \epsilon_0 c E^2 \geq \frac{\epsilon_0 c R^2 \left(\frac{4\pi^2 c^2 m_e}{\lambda^2} + e_e C_l \right)^2}{2 e_e^2}, \quad (78)$$

where λ is the laser wavelength. The gap D between the nano-rods is estimated from the critical plasma density for a given λ of the laser as

$$D \geq \sqrt{\frac{e_e^2 n_i R^2}{4\pi\epsilon_0 m_e c^2}} \lambda. \quad (79)$$

Figure 11 below shows the approximate radius R of the rods for various wavelengths λ for half ionized $p^{11}B$ required for the relative energy of $\epsilon_g^{pB} \approx 0.5$ MeV between protons and boron ions. For a given rod radius R and half ionized $p^{11}B$ the required

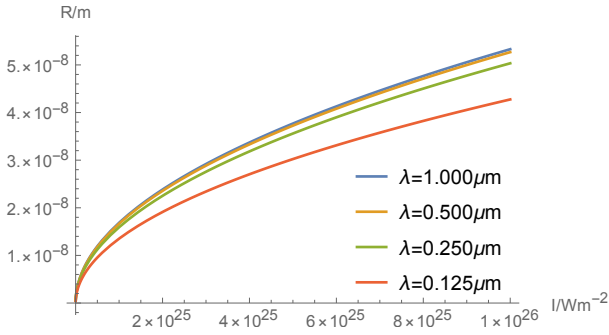


Figure 11: Nano-rod radius R versus laser intensity for a relative energy of $\epsilon_g^{pB} \approx 0.5$ MeV between protons and boron ions for various laser wavelengths for $p^{11}B$. The fuel is assumed to be half ionized.

gap D between nano-rods for stable laser pulse propagation is shown in Fig. 12.

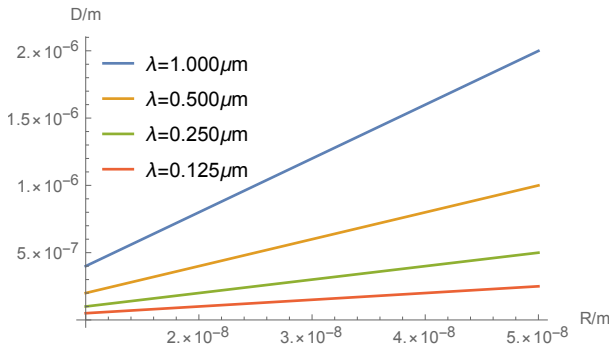


Figure 12: Inter-rod gap D versus nano-rod radius R for $p^{11}B$. The fuel is assumed to be half ionized.

The gap D , the radius R , and the charge state n_i of the rods can be engineered to match the laser driver for optimal nano-acceleration of ions. Within the scope of the model it is the goal to convert a large share of the external laser energy into ionic motion. Laser-optical instabilities have to be avoided.

Since the required intensities and charge densities are high, the power of the required laser pulses might exceed the critical power for self-focusing. However, self-focusing is suppressed for sufficiently short laser pulses with $L \leq \lambda_p$ according to [10, 11, 12], where $\lambda_p = 2\pi/k_p$ is the plasma length. We have

$$P_{c,sp} \approx \frac{2 P_c}{k_p^2 \zeta^2} \gg P_c, \quad (80)$$

$$P_c \approx 17 \frac{\omega^2}{\omega_{pe}^2} \text{GW}, \quad (81)$$

where ζ is the pulse length in the laser pulse frame. The time required to ionize the nano-rods increases $P_{c,sp}$ further and hence allows for laser pulses with $L > \lambda_p$.

The impact of secular electromagnetic fields on η^{kl} is neglected in the present paper. Since ultra-short laser pulses are capable of capturing ionizing electrons from the nano-rods, large electronic currents and return currents along the z -axis are generated which produce secular electric and magnetic fields.

Neglecting collisional and radiative resistivities in (36), we have for the electronic fluid

$$\frac{\partial n_e}{\partial t} + \frac{\partial}{\partial \vec{x}} \cdot (n_e \vec{v}_e) = 0, \quad (82)$$

$$\left(\frac{\partial}{\partial t} + \vec{v}_e \cdot \frac{\partial}{\partial \vec{x}} \right) \vec{v}_e = -\frac{q_e}{m_e} \left(\vec{E} + \vec{v}_e \times \vec{B} \right) + \frac{q_e}{m_e n_e} \frac{\partial P_e}{\partial \vec{x}}, \quad (83)$$

where

$$\frac{\partial \vec{E}}{\partial t} = \frac{\partial}{\partial \vec{x}} \times \vec{B} - \frac{1}{\epsilon_0 c^2} \vec{j}_e, \quad (84)$$

$$\frac{\partial \vec{B}}{\partial t} = -\frac{\partial}{\partial \vec{x}} \times \vec{E}, \quad (85)$$

$$\frac{\partial}{\partial \vec{x}} \cdot \vec{E} = \frac{1}{\epsilon_0} \rho, \quad (86)$$

$$\frac{\partial}{\partial \vec{x}} \cdot \vec{B} = 0. \quad (87)$$

The parameter P_e is the electronic plasma pressure. The electric and magnetic fields in (82) - (87) are slowly varying after the laser pulse has left, as simulations confirm. Assuming $d\vec{v}_e/dt \approx 0$ and piecewise constant n_e and j_e we obtain with the help of (83)

$$n_e \vec{E} + n_e \vec{v}_e \times \vec{B} - \frac{\partial P_e}{\partial \vec{x}} \approx 0, \quad (88)$$

$$\frac{\partial \vec{B}}{\partial t} = \frac{\partial}{\partial \vec{x}} \times (\vec{v}_e \times \vec{B}) \approx 0, \quad (89)$$

$$\frac{\partial}{\partial \vec{x}} \times \vec{E} \approx 0, \quad (90)$$

$$\frac{\partial}{\partial \vec{x}} \times \vec{B} \approx \frac{1}{\epsilon_0 c^2} \vec{j}_e. \quad (91)$$

The strength of the magnetic fields can be estimated if the electronic current densities are known. We approximate

$$\vec{B}(\vec{r}, t) \approx \begin{cases} \frac{j_e r}{2\epsilon_0 c^2} \vec{e}_\phi, & r \leq R_L \\ 0, & r > R_L \end{cases}, \quad (92)$$

where $j_e = e_e n_e v_e$ is the strength of the electronic current density and R_L is the effective laser pulse radius. The electric field associated with j_e and B is according to (83)

$$\vec{E}(\vec{r}, t) \approx -\frac{1}{e_e n_e} \vec{j}_e \times \vec{B}(r) + \frac{1}{m_e} \frac{\partial P_e}{\partial \vec{x}}. \quad (93)$$

The discussion of the impact of secular electromagnetic fields on η^{kl} is beyond the scope of the present paper.

In section 7 we discuss radiative energy loss to obtain a feeling for the time scales involved.

7. Radiative energy loss

Since the transport framework (6) - (9) is based on a BBGKY-hierarchy up to binary correlation order, we have radiative contributions to the equations of motion of charged particles by mean-field radiation which is traditionally called radiation reaction [13] and by radiative collisions in binary correlation order. The principal calculation of the latter is conceptually outlined in [8]. They are obtained with the help of the \mathcal{T} -matrix in (5).

Both contributions modify the equations of motion of an electron. While electrons are subject to self-radiation, binary level radiative collisions, and the impact of external fields, ions are mainly subject to radiation-free collisions and the impact of secondary collective fields, as outlined in (42) and (59) - (60). Their reactive dynamics is given by (58) - (60) or, on a very detailed level, by the underlying kinetic equations (6) - (9) that contain radiation reaction [13]. The description of radiation reaction based on the approach in [13] to a quantum level is in preparation.

Ions mainly lose their energy via collisions with electrons. As long as electrons are hot they cannot collide efficiently with cold ions. The interaction of the electrons with the external laser driver accelerates them to the speed of light. However, due to radiative energy loss electrons lose their initial energy and eventually collide with ions, thus draining the energy contained in the ionic subsystem.

The radiation loss per single electron can be estimated to be [13, 14]

$$\frac{dp^\mu}{d\tau} \approx \frac{2\tau_0}{3} \frac{m_e}{c^2} a^\nu a_\nu u^\mu, \quad \tau_0 = \frac{e^2}{4\pi\epsilon_0 m_e c^3}. \quad (94)$$

The radiation power loss per electron is given by

$$\frac{d(c p^0 - m_e c^2)}{dt} \approx \frac{2\tau_0}{3} \frac{m_e}{c^2} a^\nu a_\nu c^2, \quad (95)$$

where

$$\frac{dx^\nu}{d\tau} = u^\nu, \quad \frac{du^\nu}{d\tau} = a^\nu \approx \frac{e}{m_e} F^{\nu\alpha} u_\alpha. \quad (96)$$

According to Landau and Lifshitz [15] we have

$$a^\nu a_\nu \approx -\frac{m_e^2 c^6}{\hbar^2} \chi_e^2, \quad \chi_e = \frac{e\hbar}{m_e^2 c^3} \sqrt{-(F^{\nu\alpha} p_\alpha)^2}. \quad (97)$$

The strongest field in the fast micro-reactor is the laser field. We assume

$$\chi_e \approx \frac{\gamma E}{E_s} \approx 10^{-5}, \quad E_s = \frac{m_e^2 c^3}{e\hbar} \approx 10^{18} \frac{\text{V}}{\text{m}}. \quad (98)$$

This implies for the electronic radiation loss power density

$$I_{cl} \approx \frac{1}{6\pi} \frac{e^2 m_e^2 c^3 n_e}{\epsilon_0 \hbar^2} \chi_e^2 \approx 3.2 \cdot 10^{-7} n_e \chi_e^2 \frac{\text{J}}{\text{ps}}. \quad (99)$$

It is also possible to calculate the quantum corrections to radiation reaction including the impact of the nonlinear Compton effect according to the papers by Ritus and Nikishov [14]. The emitted integrated radiation loss power density for $\chi_e \ll 1$ according to [14] is

$$I_{RN} \approx I_{cl} \left(1 - \frac{55\sqrt{3}}{16} \chi_e + 48 \chi_e^2 \pm \dots \right) \leq I_{cl}. \quad (100)$$

Binary correlation order radiative processes cannot drain electronic energy faster than the total energy of a radiation electron multiplied by the binary collision frequency

$$\nu_{ke} \approx \frac{e_k^2 e_l^2 n_l}{4\pi\epsilon_0 m_{ke}^2 \nu_{ke}^3} \ln \Lambda_{ke}, \quad \nu_{ke} = |\vec{v}_k - \vec{v}_e|, \quad (101)$$

where k can also represent an electron. We estimate approximately $\nu_{ke} \approx (10^9 - 10^{11}) \text{s}^{-1}$ and hence electronic energy loss in the fast micro-reactor at near solid density via collisions takes about 10 - 1000 ps.

8. Summary

We propose an emergent micro-reactor concept based on very small nano-structures interacting with powerful short laser pulses for triggering nuclear fusion reactions appropriate for a range of nuclear fuels. It is driven by advanced ultra-short ultra-high energy laser pulses in the UV to the VUV wavelength range. The embedded nano-structures are quite small and represent an integrated nano-accelerator.

The micro-reactor is a concept promising efficient nuclear fuel conversion at near solid fuel density, which can be tested experimentally. The reactor proposed here should be far more efficient than traditional pitcher - catcher configurations.

With the help of the analysis of conversion fractions η^{kl} fusion enhancing configurations in emergent micro-reactors can be addressed. In the paper the conversion fraction η^{kl} for an integrated pitcher - catcher configuration has been analyzed.

Due to the availability of modern lasers the scope of fusion enhancing configurations is much wider than the one of classical confinement configurations discussed in the context of traditional fusion devices.

The present paper represents an introduction into a potentially powerful micro-reactor concept. We will follow up with this paper by a number of more detailed papers that focus on advanced fusion enhancing configurations and the associated limiting conversion fractions.

9. Acknowledgements

The present work has been motivated by the Marvel Fusion GmbH.

References

- [1] L. Fedeli, A. Formenti, L. Cialfi, A. Pazzaglia, M. Passoni, Ultra-intense laser interaction with nanostructured near-critical plasmas, *Scientific reports* 8 (1) (2018) 1–10.
- [2] D. Margarone, J. Bonvalet, L. Giuffrida, A. Morace, V. Kantarelou, M. Tosca, D. Raffestin, P. Nicolai, A. Picciotto, Y. Abe, et al., In-target proton–boron nuclear fusion using a pw-class laser, *Applied Sciences* 12 (3) (2022) 1444.
- [3] A. Curtis, C. Calvi, J. Tinsley, R. Hollinger, V. Kaymak, A. Pukhov, S. Wang, A. Rockwood, Y. Wang, V. N. Shlyaptev, et al., [Micro-scale fusion in dense relativistic nanowire array plasmas](https://doi.org/10.1038/s41467-018-03445-z), *Nature communications* 9 (1) (2018) 1–7. doi:<https://doi.org/10.1038/s41467-018-03445-z>. URL <https://www.nature.com/articles/s41467-018-03445-z>
- [4] C. G. Van Weert, W. Van Leeuwen, S. De Groot, [Elements of relativistic kinetic theory](https://doi.org/10.1016/0031-8914(73)90082-7), *Physica* 69 (2) (1973) 441–457. doi:[https://doi.org/10.1016/0031-8914\(73\)90082-7](https://doi.org/10.1016/0031-8914(73)90082-7). URL [https://doi.org/10.1016/0031-8914\(73\)90082-7](https://doi.org/10.1016/0031-8914(73)90082-7)
- [5] D. Vasak, M. Gyulassy, H.-T. Elze, [Quantum transport theory for abelian plasmas](http://dx.doi.org/10.1016/0003-4916(87)90169-2), *Annals of Physics* 173 (2) (1987) 462 – 492. doi:[http://dx.doi.org/10.1016/0003-4916\(87\)90169-2](http://dx.doi.org/10.1016/0003-4916(87)90169-2). URL <http://www.sciencedirect.com/science/article/pii/S0003491687901692>
- [6] P. Zhuang, U. Heinz, [Relativistic quantum transport theory for electrodynamics](http://dx.doi.org/10.1006/aphy.1996.0011), *Annals of Physics* 245 (2) (1996) 311 – 338. doi:<http://dx.doi.org/10.1006/aphy.1996.0011>. URL <http://www.sciencedirect.com/science/article/pii/S0003491696900111>
- [7] C. G. van Weert, W. de Boer, [On the derivation of quantum kinetic equations. i. collision expansions](https://doi.org/10.1007/BF01018093), *Journal of Statistical Physics* 18 (3) (1978) 271–280. doi:<https://doi.org/10.1007/BF01018093>. URL <https://doi.org/10.1007/BF01018093>
- [8] B. King, H. Ruhl, [Trident pair production in a constant crossed field](https://doi.org/10.1103/PhysRevD.88.013005), *Physical Review D* 88 (1) (2013) 013005. doi:<https://doi.org/10.1103/PhysRevD.88.013005>. URL <https://journals.aps.org/prd/abstract/10.1103/PhysRevD.88.013005>
- [9] W. Nevins, R. Swain, The thermonuclear fusion rate coefficient for p-11b reactions, *Nuclear fusion* 40 (4) (2000) 865.
- [10] E. Esarey, P. Sprangle, J. Krall, A. Ting, [Self-focusing and guiding of short laser pulses in ionizing gases and plasmas](https://doi.org/10.1109/3.641305), *IEEE journal of quantum electronics* 33 (11) (1997) 1879–1914. doi:<https://doi.org/10.1109/3.641305>. URL <https://ieeexplore.ieee.org/abstract/document/641305>
- [11] P. Sprangle, E. Esarey, J. Krall, G. Joyce, [Propagation and guiding of intense laser pulses in plasmas](https://doi.org/10.1103/PhysRevLett.69.2200), *Physical review letters* 69 (15) (1992) 2200. doi:<https://doi.org/10.1103/PhysRevLett.69.2200>. URL <https://journals.aps.org/prl/abstract/10.1103/PhysRevLett.69.2200>
- [12] J. Faure, V. Malka, J.-R. Marquès, P.-G. David, F. Amiranoff, K. Ta Phuoc, A. Rousse, [Effects of pulse duration on self-focusing of ultra-short lasers in underdense plasmas](https://doi.org/10.1063/1.1447556), *Physics of Plasmas* 9 (3) (2002) 756–759. doi:<https://doi.org/10.1063/1.1447556>. URL <https://aip.scitation.org/doi/abs/10.1063/1.1447556>
- [13] C. Bild, D.-A. Deckert, H. Ruhl, [Radiation reaction in classical electrodynamics](https://doi.org/10.1103/PhysRevD.99.096001), *Physical Review D* 99 (9) (2019) 096001. doi:[10.1103/PhysRevD.99.096001](https://doi.org/10.1103/PhysRevD.99.096001). URL <https://doi.org/10.1103/PhysRevD.99.096001>
- [14] A. Nikishov, V. Ritus, Quantum processes in the field of a plane electromagnetic wave and in a constant field, *Soviet Physics JETP* 19 (5) (1964).
- [15] L. D. Landau, E. M. Lifschitz, A. Kühnel, [Lehrbuch der theoretischen Physik, 10 Bde., Bd.4, Quantenelektrodynamik](http://amazon.com/o/ASIN/3817113293/), Deutsch (Harri), 1991. URL <http://amazon.com/o/ASIN/3817113293/>